Electronic structure, stability, and strength of Cu–NiAl alloys: Experiment and DFT investigation

Zakaryaa Zarhri*

CONACYT-Tecnológico Nacional de México/I.T. Chetumal; Insurgentes 330, C.P. 77013, Chetumal, Quintana Roo, Mexico

Article info

Abstract

In this study, the copper doping effect on the NiAl structural stability, strength, and electronic structure was investigated. The samples were prepared using induction melting at 2073 K. This material presents good mechanical and physical properties such as high-temperature strength, fatigue or impact, and corrosion resistance which meet technical requirements of many applications. The microstructure of the Cu-doped nickel aluminide was studied using a metallurgical microscope and its lattice parameter was also studied and characterized using an X-ray diffractometer for different concentrations of Cu. The lattice constant of the existing phases was calculated, and it was found that the lattice distortion and gamma prime phase energy have high values allowing the increase of the entropy term of the alloy and subsequently increasing its hardness. From the ab-initio calculation, it was determined that the Cu atoms have the Al sites as a preferred site and prefer to bond with Ni atoms which leads to the improvement of the material hardness. Ab-initio density functional theory was applied to study the formation energy that revealed increasing with Cu amount.

1. Introduction

NiAl alloys are one of the most important high-temperature intermetallic compounds due to the many advantages they offer. They have several unique properties: significant payoffs as structural materials in gas turbine applications thanks to high melting temperature and high thermal conductivity that allow them to be used in a variety of specialized applications [1].

Aluminium compounds are very successful and used in numerous applications from commodity roles to modern building and construction [2]. Indeed, they are known for some properties that make them appropriate building construction materials and then, they have become important construction materials for all sorts of buildings along with steel, brick, and cement.

At high temperatures, NiAl alloys may retain stiffness and strength. Transition metals like Fe, Ni, Nb, Ti, and Co-doped NiAl are ordered intermetallic alloys that have good resistance to sulfidation, corrosion, and oxidation at room temperature or higher [3].

NiAl alloys are expected to be promising structural materials due to their high melting point [4]. Porcayo-Calderon *et al*. investigated the effect of the Cu addition on a corrosion performance of the Ni_3Al intermetallic alloy in sulfuric acid at low temperature [5]. It has also been reported that the addition of elements like Cu, Co, Ti, and Fe can improve the mechanical properties of Ni–Al intermetallics [6, 7] and also electrical properties [8]. Other works revealed that small additions of transition metal may significantly enhance the room temperature ductility of NiAl single crystals or other materials [9–13].

Moreover, the NiAl intermetallic compound is applicable in the aerospace industry thanks to its strength and good oxidation resistance at high temperatures [14]. Uncontrollable factors such as impurity content, heat treatment, constitutional defects, or surface conditions influence experimental investigations of the mechanical properties [7]. Also, a considerable amount of scattering in ductility is usually observed in experiments [8].

*Corresponding author at: z.zarhri@gmail.com

Additionally, metals have important magnetic properties. However, experimental information is limited when magnetism at the atomic level is of concern.

In this paper, NiAl and Cu-doped NiAl were melted at a high temperature to study the mechanical and physical properties of these alloy samples at different concentrations of copper doping. In addition, an ab-initio simulation helped investigate the material behaviour at a low scale. The ab-initio density functional theory approach has many advantages, in particular the ability to calculate properties of a paramagnetic Cu–NiAl alloy with large-scale supercells.

2. Synthesis and characterization

Cu–NiAl was synthesized by the induction melting method using appropriate amounts of Cu, Ni, and Al elements by calculating the exact weight corresponding to a desired number of atoms of each compound and its contribution to the unit cell.

The recipient of graphene under a temperature of above 2073 K and atmospheric pressure was used. The samples were remelted several times to ensure homogeneity [15].

Alloys were produced in quartz crucibles with an induction furnace in an inert atmosphere from elements of high purity. Ingots were cooled and subsequently solidified inside the crucibles in the furnace at room temperature and in this condition they were used in the studies.

The X-ray diffraction (XRD) of all samples was made with a Bruker D8 Advance X-ray using Cu-Kα radiation (1.5406 Å) at 30 kV accelerating voltage and a 20 mA current. The samples were scanned at 2θ for angles from 20° to 95°, with a 0.015 step.

3. NiAl structure and ab-initio calculations

NiAl structure is a face centred cubic with a space group of 221/pm-3m and atoms position (0, 0, 0) and (½, ½, ½), respectively for nickel and aluminium. The lattice parameter used in the electronic structure study is the one found by the X-Ray diffraction (2.887 Å). The electronic structure analysis of all the compounds was carried out using the DFT framework within the MACHIKANEYAMA2002V09 package based on Korringa-Kohn-Rostoker (KKR) method [16, 17]. In the study, the exchange–correlation functional was used combined with the coherent potential approximation (CPA) and the local density approximation (LDA) [18], as well as the generalized gradient approximation (GGA) para-meterized by Perdew Burke Ernzerhof (PBE) [19], which is one of the most widely used functionals in calculations involving solids [20]. This ab-initio method is well known in the investigation of the material physical and chemical properties [21–25].

4. Results and discussion

From the X-Ray diffraction of Cu-doped NiAl at 10% of copper and 5% of aluminium [Fig. 1(a)], the peaks revealed an interatomic distance of 2.887 Å. which was compared to the JCPDS database to confirm the quality of the found results of the Miller indices. It confirmed the incorporation of copper in the tested material. The difference between the interatomic distance and the lattice parameter successively compared to the database is due to the large radius difference between copper and aluminium. This implies the existence of other phases where copper
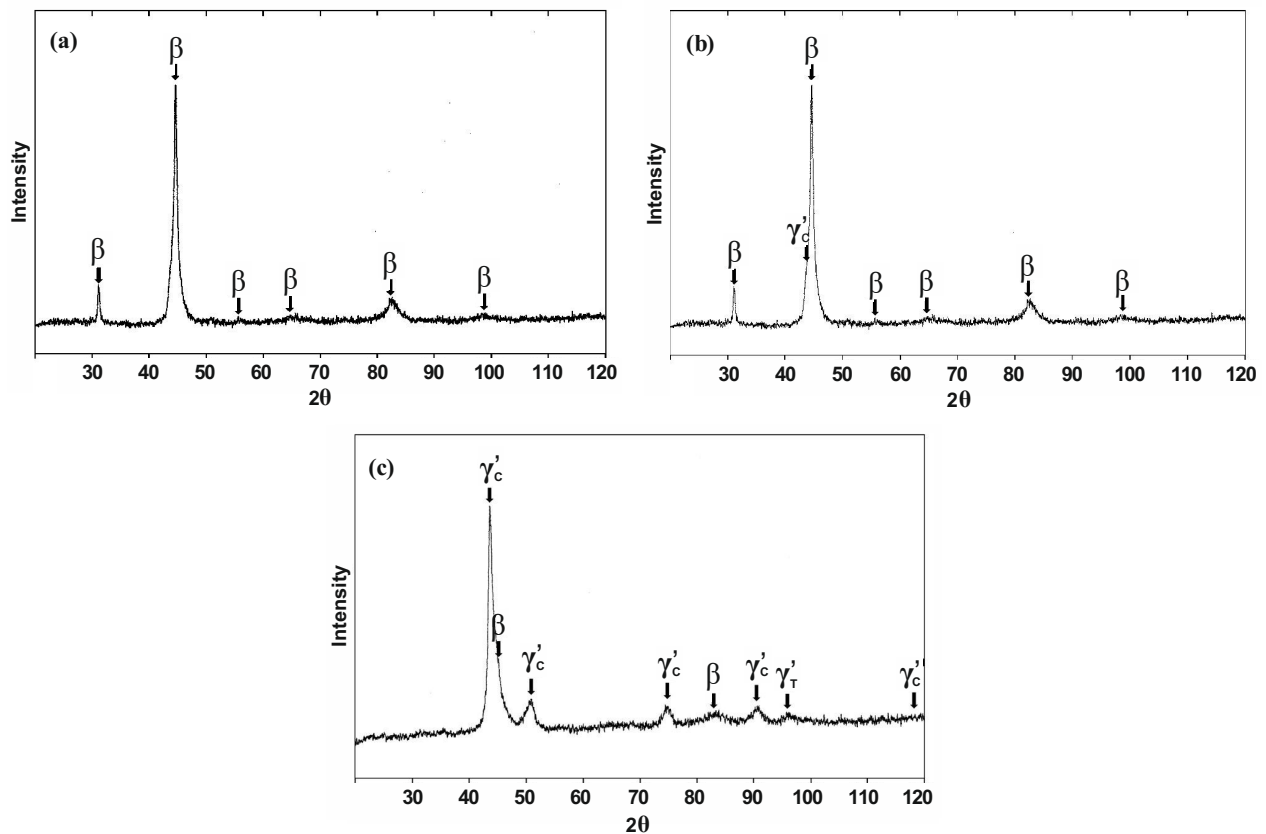

Fig. 1. X-ray diffraction of Cu–NiAl samples: $NiAl_{0.8}Cu_{0.2}$ (a), $NiAl_{0.7}Cu_{0.3}$ (b), and $NiAl_{0.6}Cu_{0.4}$ (c).

took place of aluminium because it prefers to bond with nickel: this will be confirmed by using the first-principle calculations by computing the total and formation energies for each case of Cu-doped NiAl where Cu may occupy different sites.

The X-ray pattern shows that it corresponds to an alloy formed from the NiAl type. Taking the Cu-doped NiAl system phase equilibrium diagram as a reference, an alloy with a 5% Cu content corresponds to a monophasic alloy constituted by the Ni-rich β-NiAl phase. In the NiAl system, the intermetallic compound of NiAl corresponds to a B2-type crystal structure that crystallizes in the primitive cubic structure of the CsCl type. The composition of 50% Ni and 50% Al is an alloy called stoichiometric with a cell parameter equal to 2.887 Å and a density of 5.9 g/cm^3. The XRD pattern shown in Fig. 1(a) corresponds to a NiAl alloy with 10% at Cu. The indexing done of the diffraction peaks corresponds to the β-NiAl phase. Compared with the stoichiometric alloy, a slight decrease in the mesh parameter was observed (2.881 Å).

The diffraction pattern of Fig. 1(b) corresponds to the alloy with 15% Cu and 15% Al while Fig. 1(c) is for the alloy with 20% Cu and 20% Al. The indexing corresponds to a biphasic alloy constituted mainly by the phase γ'-Ni$_3$Al which coexists with the β-NiAl phase. This result corresponds to the position within the phase diagram for the mentioned alloy. The diffraction peaks correspond mainly to the predominant phase of γ'-Ni$_3$Al which suggests that it is in a larger quantity due to the intensity and presence of its peaks and the proximity of the single-phase field of γ'-Ni$_3$Al. According to the JCPDS card, the intensity of the peaks (110) and (220) was considerably more intense than that of the main peaks (111) and (200). The calculated lattice parameter of the alloy composition was 3.572 Å, which is in agreement with that reported in the literature for Ni$_3$Al [26, 27].

At a higher percentage of copper, the grains present in the alloy [Fig. 1(b)] consist of multiple phases which belong to the Ni-rich side [28, 29]. This can be observed in the metallurgical images in Figs. 2(a), 2(b), and 2(c). However, even when it is not possible to appreciate it with the naked eye, in these diffractograms, there is a displacement of the representative peaks towards smaller angles. This variation is directly proportional to the Cu increase in the alloys.

Macro-hardness and micro-hardness tests, successively Rockwell and Vickers hardness tests (Table 1), were preceded with different hardness tests for all samples to check the influence of doping on the hardness of the tested material.

Table 1
Rockwell and Vickers hardness tests of
the tested binary and ternary alloys.

Cu (%)	Hardness test	
	Rockwell (HR)	Vickers (HV)
0	23 ± 0.69	301 ± 15.05
5	25 ± 0.75	302 ± 15.1
10	27 ± 0.81	311 ± 15.55
15	29 ± 0.87	321 ± 16.05
20	33 ± 0.99	344 ± 17.2
25	36 ± 1.08	400 ± 20

The principle of hardness testing consists of pressing a hard indenter with an exactly defined force onto the test piece, then evaluating the surface area of the indentation. The hardness of the sample is equal to the test force divided by the surface area of the indentation.

It can be seen from Table 1 that the hardness increases as the copper concentration increases. This is due to the
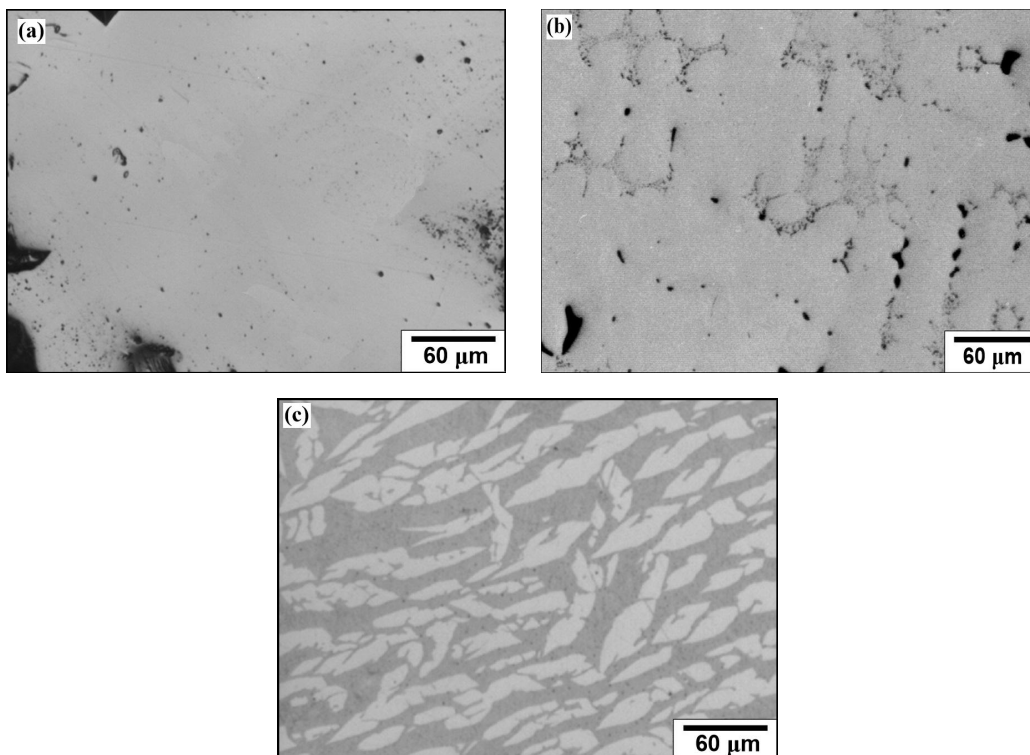

Fig. 2. Metallurgical microscope images of: NiAl$_{0.8}$Cu$_{0.2}$ (a), NiAl$_{0.7}$Cu$_{0.3}$ (b), and NiAl$_{0.6}$Cu$_{0.4}$ (c).

incorporation of copper in the tested material which is in place of Al, and because the radius difference between copper and nickel is not large, this makes the structure more stable and then increases the hardness of the material.

5. The formation energy and the system stability

The initial parameter ($a = 2.887$ Å) was used for the simulation calculations which was found by analysing the X-Ray diffraction patterns, then, the unit cell was relaxed to find the optimal structure. The relaxation method consists of varying the lattice parameter and calculating the corresponding total energy to find the minimum energy that corresponds to the most stable state of the host material. The equilibrium lattice constant is the one that corresponds to the minimum energy (Fig. 3).
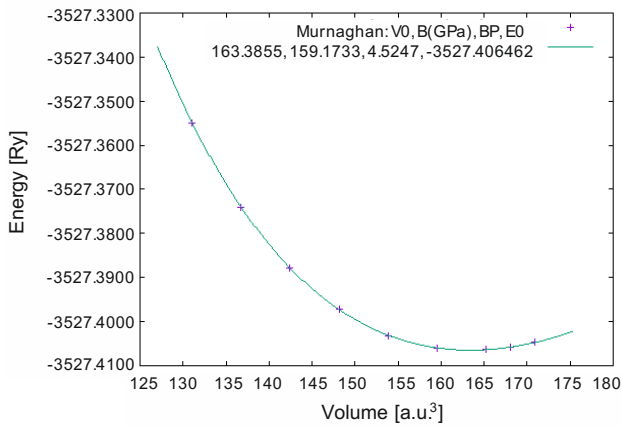

Fig. 3. Structure parameters optimization of a NiAl unit cell (Relaxation).

Formation energy (ΔE) is a very important parameter to identify the system stability, the feasibility of the alloy, and, also, the classification of hydrogen storage materials. It is also used to determine the heat of hydrogen reaction and deduce the temperature of hydrogen desorption in the material, and the fracture energy that depends on the deviations of a real crack from an idealized crack plane for a high strength concrete simulation that can be controlled to achieve the necessary durability of concrete structures [30]. The formation energies have been evaluated by the following formula for the Cu-doped system [31]

$$\Delta E = E_{tot}(\text{ternary or binary alloy}) - \sum E_{tot}(\text{reactants}) \quad (1)$$

$$\Delta E\big(\text{NiAl}_{(1-x)}\text{Cu}_x\big) = E\big(\text{NiAl}_{(1-x)}\text{Cu}_x\big) - E_{pure}(\text{NiAl}) + xE(\text{Al}) - xE(\text{Cu}) \quad (2)$$

$$\Delta E\big(\text{Ni}_{(1-x)}\text{Cu}_x\text{Al}\big) = E\big(\text{Ni}_{(1-x)}\text{Cu}_x\text{Al}\big) - E_{pure}(\text{NiAl}) + xE(\text{Ni}) - xE(\text{Cu}) \quad (3)$$

$E(\text{Ni}_{(1-x)}\text{Cu}_x\text{Al})$ is the total energy of the ternary alloy, $E_{pure}(\text{NiAl})$ is the total energy of the bulk NiAl without doping, and $E(\text{Ni})$, $E(\text{Al})$, and $E(\text{Cu})$ are respectively the chemical potentials of Ni, Al, and Cu unit cells in their reference states.

The calculated formation energies, with x varying from 0.05 to 0.25, are summarized in Table 2. These results

indicate higher stability in the case of $\text{NiAl}_{(1-x)}\text{Cu}_x$ compared to $\text{Ni}_{(1-x)}\text{Cu}_x\text{Al}$ system.

Cu-doped NiAl has lower energies when Cu is in Al sites which is related to the most stable state. This means that copper prefers to bond with nickel atoms due to the electrostatic attractive forces between delocalized electrons and positively charged metal ions. When the copper concentration is higher, the formation energy is lower. As noticed in previous works, the hydrogen atoms prefer to bond with nickel instead of aluminium [32].

Table 2
Total and formation energies of Cu-doped NiAl by DFT calculations.

Cu (%)	Total energy (Ry)		Formation energy (eV)	
	Cu in Al sites	Cu in Ni sites	Cu in Al sites	Cu in Ni sites
5	−3802.6167294	−3547.3472522	−8.03	−7.65
10	−4084.6945317	−3574.1552411	−8.47	−7.71
15	−4366.7732641	−3600.9628534	−8.91	−7.76
20	−4648.8532459	−3627.7702108	−9.35	−7.81
25	−4930.9338289	−3654.5775393	−9.78	−7.86

Figure 4 shows the density of state of the tested alloys. A shift of the valance and the conduction bands to higher energy can be noticed. This is due to the addition of new states which allow the excitation of electrons from the VB to the CB.
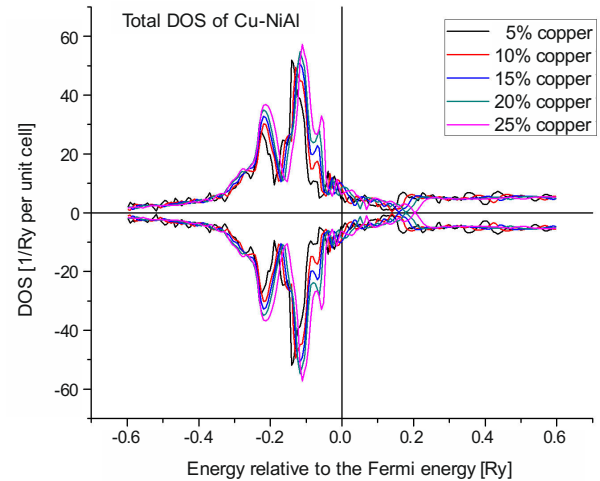

Fig. 4. Densities of states of different concentrations of Cu-doped NiAl where doping is in Al sites.

A zero magnetic moment was found and confirmed by the up and down spins symmetry in valence and conduction bands. Doping the system caused it to try finding an equilibrium of the electronic density which in this case is the position of symmetry.

It is estimated that there are from 10 million to 1 billion dislocations per square centimeter in a metal, and each dislocation has a strain field associated with it. These dislocations are the cause of the fracture of the bulk material.

The addition of other elements to the tested material contributes to strengthening its solid solution. The added

elements can be located between the atoms of the bulk material or replace the atoms; this is called interstitial or substitutional solid solution which causes a distortion in the atomic structure of the material. This distortion interacts with the dislocations preventing their movement and then strengthening the sample. Improvement in hardness can be achieved due to lattice distortion strengthening and higher anti-phase boundary energy of gamma prime [33].

6. Conclusions

Cu-doped NiAl was synthesized using induction melting at a temperature above 2073 K. The X-ray diffraction confirms the incorporation of copper in the tested binary alloy. It has been shown that copper prefers to bond with nickel and then it is located in aluminium sites. This was confirmed by computing and calculating the total and formation energy using ab-initio and DFT method where it was found out that these energies are minimal when Cu takes Al sites. The addition of copper in the NiAl alloy increases the material hardness.

The lattice distortion and gamma prime phase energy have high values which allowed the increase of the entropy term of the alloy and subsequently increased its hardness.

Acknowledgements

References

[1] Bochenek, K. & Basista, M. Advances in processing of NiAl intermetallic alloys and composites for high temperature aerospace applications. *Prog. Aerosp. Sci.* **79**, 136–146 (2015). https://doi.org/10.1016/j.paerosci.2015.09.003

[2] Chandler, K. A., *Marine and Offshore Corrosion*. (Elsevier, 1985). https://doi.org/10.1016/C2013-0-06267-6

[3] Busso, E. P. & McClintock, F. A. Mechanisms of cyclic deformation of NiAl single crystals at high temperatures. *Acta Metall. Mater.* **42**, 3263–3275 (1994). https://doi.org/10.1016/0956-7151(94)90459-6

[4] Ren, W. L., Guo, J. T., Li, G. S. & Wu, J. S. The critical temperature for brittle-to-ductile transition of intermetallic compound based on NiAl. *Mater. Lett.* **58**, 1272–1276 (2004). https://doi.org/10.1016/j.matlet.2003.09.020

[5] Porcayo-Calderon, J. *et al.* Effect of Cu addition on the electrochemical corrosion performance of Ni₃Al in 1.0 M H₂SO₄. *Adv. Mater. Sci. Eng.* **2015**, 209286 (2015). https://doi.org/10.1155/2015/209286

[6] Huai, K., Guo, J., Gao, Q. & Yang, R. The microstructure of Au-doped NiAl–Cr(Mo) eutectic and its mechanical properties. *Mater. Lett.* **59**, 3291–3294 (2005). https://doi.org/10.1016/j.matlet.2005.05.061

[7] Chiba, A., Hanada, S. & Watanabe, S. Improvement in ductility of Ni₃Al by γ former doping. *Mater. Sci. Eng. A* **152**, 108–113 (1992). https://doi.org/10.1016/0921-5093(92)90054-5

[8] Bhosale, A. G. & Chougule, B. K. Electrical conduction in Ni–Al ferrites. *Mater. Lett.* **60**, 3912–3915 (2006). https://doi.org/10.1016/j.matlet.2006.03.139

[9] Darolia, R., Lahrman, D. & Field, R. The effect of iron, gallium and molybdenum on the room temperature tensile ductility of NiAl. *Scr. Metall. Mater.* **26**, 1007–1012 (1992). https://doi.org/10.1016/0956-716X(92)90221-Y

[10] Pan, Y., Li, Y. & Zheng, Q. Influence of Ir concentration on the structure, elastic modulus and elastic anisotropy of NbIr based compounds from first-principles calculations. *J. Alloys Compd.* **789**, 860–866 (2019). https://doi.org/10.1016/j.jallcom.2019.03.083

[11] Pan, Y., Wang, P. & Zhang, C.-M. Structure, mechanical, electronic and thermodynamic properties of Mo₅Si₃ from first-principles calculations. *Ceram. Int.* **44**, 12357–12362 (2018). https://doi.org/10.1016/j.ceramint.2018.04.023

[12] Pan, Y. First-principles investigation of the new phases and electrochemical properties of MoSi₂ as the electrode materials of lithium ion battery. *J. Alloys Compd.* **779**, 813–820 (2019). https://doi.org/10.1016/j.jallcom.2018.11.352

[13] Pan, Y., Wang, S., Zhang, X. & Jia, L. First-principles investigation of new structure, mechanical and electronic properties of Mo-based silicides. *Ceram. Int.* **44**, 1744–1750 (2018). https://doi.org/10.1016/j.ceramint.2017.10.106

[14] Huang, J., Xing, H., Wen, Y. & Sun, J. Effect of Fe ternary addition on ductility of NiAl intermetallic alloy. *Rare Met.* **30**, 316–319 (2011). https://doi.org/10.1007/s12598-011-0292-7

[15] Sugilal, G. *et al.* Indigenous development of induction skull melting technology for electromagnetic processing of refractory and reactive metals and alloys. *Mater. Today Proc.* **3**, 2942–2950 (2016). https://doi.org/10.1016/j.matpr.2016.09.007

[16] Akai, H. Fast Korringa-Kohn-Rostoker coherent potential approximation and its application to FCC Ni-Fe systems. *J. Phys. Condens. Matter* **1**, 8045–8064 (1989). https://doi.org/10.1088/0953-8984/1/43/006

[17] Nagy, Á. Density functional. Theory and application to atoms and molecules. *Phys. Rep.* **298**, 1–79 (1998). https://doi.org/10.1016/S0370-1573(97)00083-5

[18] Zarhri, Z., Ziat, Y., El Rhazouani, O., Benyoussef, A. & Elkenz, A. Titanium atoms dimerization phenomenon and magnetic properties of titanium-antisite (Ti₀) and chromium doped rutile TiO₂, ab-initio calculation. *J. Phys. Chem. Solids* **94**, 12–16 (2016). https://doi.org/10.1016/j.jpcs.2016.03.002

[19] Perdew, J. P., Burke, K. & Ernzerhof, M. Generalized gradient approximation made simple. *Phys. Rev. Lett.* **77**, 3865–3868 (1996). https://doi.org/10.1103/PhysRevLett.77.3865

[20] Zarhri, Z. *et al.* Ab-initio study of magnetism behavior in TiO₂ semiconductor with structural defects. *J. Magn. Magn. Mater.* **406**, 212–216 (2016). https://doi.org/10.1016/j.jmmm.2016.01.029

[21] Pan, Y. & Wen, M. Noble metals enhanced catalytic activity of anatase TiO₂ for hydrogen evolution reaction. *Int. J. Hydrogen Energy* **43**, 22055–22063 (2018). https://doi.org/10.1016/j.ijhydene.2018.10.093

[22] Pan, Y., Li, Y. Q., Zheng, Q. H. & Xu, Y. Point defect of titanium sesquioxide Ti₂O₃ as the application of next generation Li-ion batteries. *J. Alloys Compd.* **786**, 621–626 (2019). https://doi.org/10.1016/j.jallcom.2019.02.054

[23] Pan, Y. Theoretical discovery of high capacity hydrogen storage metal tetrahydrides. *Int. J. Hydrogen Energy* **44**, 18153–18158 (2019). https://doi.org/10.1016/j.jallcom.2019.02.054

[24] Pan, Y. Vacancy-enhanced cycle life and electrochemical performance of lithium-rich layered oxide Li₂RuO₃. *Ceram. Int.* **45**, 18315–18319 (2019). https://doi.org/10.1016/j.ceramint.2019.06.044

[25] Ziat, Y., Hammi, M., Zarhri, Z., Laghlimi, C. & El Rhazouani, O. Ferrimagnetism and ferromagnetism behavior in (C, Mn) co-doped SnO₂ for microwave and spintronic: Ab initio investigation. *J. Magn. Magn. Mater.* **483**, 219–223 (2019). https://doi.org/10.1016/j.jmmm.2019.03.084

[26] Liu, J., Cao, J., Lin, X., Song, X. & Feng, J. Microstructure and mechanical properties of diffusion bonded single crystal to polycrystalline Ni-based superalloys joint. *Mater. Des.* **49**, 622–626 (2013). https://doi.org/10.1016/j.matdes.2013.02.022

[27] Zheng, L., Sheng, L. Y., Qiao, Y. X., Yang, Y. & Lai, C. Influence of Ho and Hf on the microstructure and mechanical properties of NiAl and NiAl-Cr(Mo) eutectic alloy. *Mater. Res. Express* **6**, 046502 (2019). https://doi.org/10.1088/2053-1591/aaf8ea

[28] Sheng, L. Y. *et al.* Microstructure characteristics and compressive properties of NiAl-based multiphase alloy during heat treatments. *Mater. Sci. Eng. A* **528**, 8324–8331 (2011). https://doi.org/10.1088/2053-1591/aaf8ea

[29] Sheng, L. *et al.* Effect of Au addition on the microstructure and mechanical properties of NiAl intermetallic compound. *Intermetallics* **18**, 740–744 (2010). https://doi.org/10.1016/j.intermet.2009.10.015

[30] Wittmann, F. H. Crack formation and fracture energy of normal and high strength concrete. *Sadhana* **27**, 413–423 (2002). https://doi.org/10.1007/BF02706991

[31] Ziat, Y. *et al.* First-principles study of magnetic and electronic properties of fluorine-doped $Sn_{0.98}Mn_{0.02}O_2$ system. *J. Supercond. Novel Magn.* **29**, 2979–2985 (2016). https://doi.org/10.1007/s10948-016-3609-9

[32] Han, Y.-J. & Park, S.-J. Influence of nickel nanoparticles on hydrogen storage behaviors of MWCNTs. *Appl. Surf. Sci.* **415**, 85–89 (2017). https://doi.org/10.1016/j.apsusc.2016.12.108

[33] Tsao, T.-K. & Yeh, A.-C. The thermal stability and strength of highly alloyed Ni_3Al. *Mater. Trans.* **56**, 1905–1910 (2015). https://doi.org/10.2320/matertrans.M2015298